Progress In Electromagnetics Research B, Vol. 20, 337–352, 2010

INDUCTANCE COMPARISON OF THE SOLENOIDAL COIL OF MODULAR TOROIDAL COILS USING THE ANALYTICAL AND FINITE ELEMENT METHOD

M. R. Alizadeh Pahlavani and H. A. Mohammadpour

Department of Electrical Engineering
Iran University of Science and Technology (IUST)
Tehran, Iran

Abstract—The modular toroidal coil (MTC) is composed of several solenoidal coils (SCs) connected in series and distributed in toroidal and symmetrical forms. In this paper, we present an accurate approach for calculation of the mutual and self-inductance between all the SCs of MTC with any arbitrary section. We use Biot-Savart's and Neumann's equations to calculate the self- and mutual inductance between two filamentary circular rings with inclined axes that lie in the same plane, respectively. Their centers are either displaced along the axis of one coil or displaced along one axis of the first coil and then displaced sideways. We use the extended three-point Gaussian algorithm to solve the numerical analysis of the integrations resulting from these equations. Additionally, we apply the filament method to calculate the inductance of the MTC coil. Moreover, the finite element method (FEM) is employed to obtain SC inductance. The results obtained using the FEM confirms the analytical and empirical results. Furthermore, the comparison of the behavior of SC inductance, when the dimensional parameters of the SC are changed, with the FEM results shows an error of less than 0.2%. In this approach, we clarify how the presented equations have to be used for different coil combinations in the filament treatment. Thus, the presented approach can be easily used to calculate the mutual and self-inductance of a MTC between any two MTC rings in three dimensions.

Corresponding author: M. R. Alizadeh Pahlavani (Mr_alizadehp@iust.ac.ir).

1. INTRODUCTION

An inductive link consists of two coils, forming a loosely coupled transformer. Recent research work in the area of plasma reactors (e.g., tokamak), superconductor magnetic energy storage (SMES), and nuclear fusion reactors has been conducted on different coils [1–3]. Tokamak reactors consist of coils with different structures, such as the modular toroidal coil (MTC), the helical toroidal coil, the solenoidal coil (SC), and the poloidal coil, as seen in Fig. 1 [4]. The MTC is composed of several SCs connected in series and distributed in toroidal and symmetrical form. An SC consists of several coaxial circular rings. Each two rings of an SC, which are coaxial, or two different SCs, which are non-coaxial, can make an inductive link. The primary ring generates a magnetic field that is partly picked up by the secondary ring. In this way, power can be transferred wirelessly. The decrease in power transfer efficiency of the inductive power system is caused by lower mutual inductance due to misalignment of the rings. Therefore, in the equations of mutual inductance between two rings, misalignments have to be taken into consideration. Many contributions have been made in the literature to the problem of mutual inductance calculation for coaxial circular coils [5–11]. These contributions have been based on the application of Maxwell's formula, Neumann's formula, and the Biot–Savart law. The mutual inductance of circular rings can be obtained in analytical or semi-analytical forms expressed over elliptical integrals of the first, second, and third kind, Heuman's Lambda function, Bessel functions, and Legendre functions [12, 13]. However, the calculation of the mutual inductance of non-coaxial circular rings is of fundamental practical interest to electrical engineers and physicists. In this paper, we will present

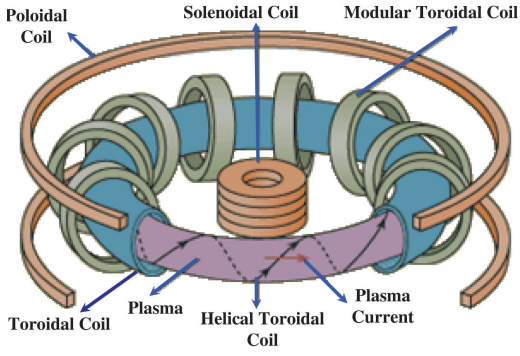

Figure 1. A typical Tokamak reactor.

the mutual inductance between two coaxial rings and two non-coaxial rings. This is accomplished by defining a new coordinate system and using Neumann's equations. Additionally, the self-inductance of a ring in this coordinate system is derived using Biot-Savart equation. Finally, we will use the filament method [14, 15] to calculate the self-inductance of an SC or the mutual inductance of two SCs. These SCs may have any cross-section. Note that the problem is purely 3-D because SCs' axes may be coaxial or non-coaxial. In this paper, we use extended 3-point Gaussian numerical integration to solve the presented equations. They are validated using the finite element method (FEM).

This paper is organized as follows: In Section 2, the MTC and some definitions are introduced. In Section 3, an appropriate coordinate system to simplify the mathematical equations is presented, the longitudinal components of the rings element of each SC in this coordinate system are introduced, and the relations between the geometrical parameters of the Kth SC with the geometrical parameters of the rings located in the same coil are derived. In Section 4, equations for the calculation of the self-inductance of one ring, the mutual inductance of two rings, and the inductance matrices of the SCs and the MTC are presented. In Section 5, the analytical results of the inductances of one and two rings are compared with the corresponding empirical results. In Section 6, a comparison is made between the FEM results and analytical results of the inductance of an SC.

2. THE MTC AND SOME DEFINITIONS

The structure of MTC is shown in Fig. 2. As observed, this structure is composed of S SCs connected in series distributed in toroidal and the symmetrical forms. In this figure, S is assumed to be equal to 8. In Fig. 2(b), the projection of this coil on x-y plane is shown. In this figure, R_{mk} is the distance between the symmetry center of the Kth SC from the z-axis. Additionally, the angle between the R_{mk} direction and the latitudinal axis of the Kth SC is shown by υ_{mk}.

Moreover, the toroidal angle of the Kth SC is defined by φ_{mk}, and the distance between the longitudinal axis of the Kth SC and plane $z = 0$ is shown by H_{mk}. As mentioned above, in the MTC, the values of R_{mi} and υ_{mi}, $i = 1, \ldots, S$ are defined as $R_{mi} = \text{const}$, $\upsilon_{mi} = 0$.

The dependency of analytical equations of inductance of the MTC on the geometrical parameters of the SCs, such as R_{mi}, υ_{mi}, φ_{mi}, H_{mi}, and $i = 1, \ldots, S$, when the dimensional parameters of the SCs are known, shows that these parameters can be used as the degrees of freedom of the objective function and thus can be manipulated to satisfy the optimization function.

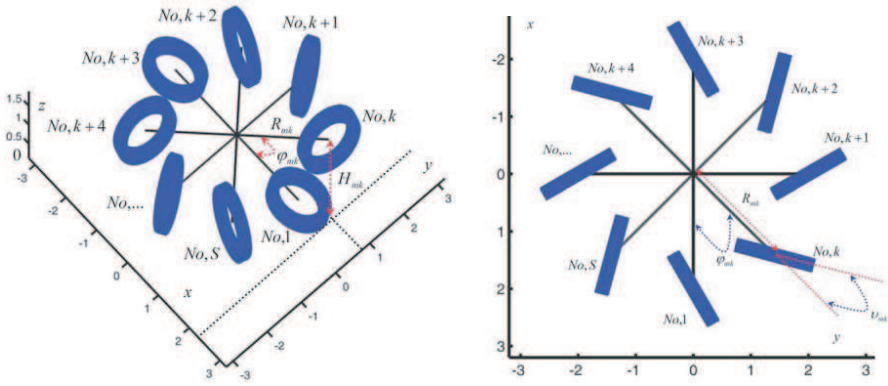

Figure 2. The structure of a modular toroidal coil with 8 solenoid coils. (a) 3D diagram of the modular toroidal coil. (b) Projection of the structure of the modular toroidal coil on the x-y plane.

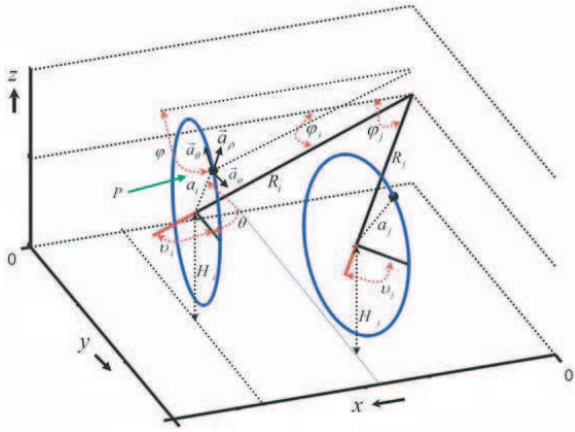

Figure 3. The coordinate system and the two hypothetical rings of the modular toroidal coil.

3. COORDINATE SYSTEM AND LONGITUDINAL COMPONENTS

Figure 3 shows the ith and the jth hypothetical rings of the MTC with the geometrical parameters of υ_i, φ_i, R_i, a_i, H_i and υ_j, φ_j, R_j, a_j, H_j, respectively. To consider these parameters, the coordinate system should be non-orthogonal, 3D, and rotationalin

order to simplify the mathematical equations. An arbitrary point P in the space is defined by ρ, θ, and φ (see Fig. 3). In this coordinate system, it is typical to use $\vec{a}_\rho$, $\vec{a}_\theta$, and $\vec{a}_\varphi$ to represent unit vectors in directions ρ, θ, and φ, respectively. In Fig. 3, the unit vectors of this coordinate system for point P, located on the ith coil, is shown. The Cartesian coordinate system of this point can be expressed as Equations (1)–(3) using the projection of the ith ring on the x-y plane, as shown in Fig. 4. The longitudinal components of this coordinate system are defined by Equation (4).

$$x_P = (R_i \operatorname{Cos}(\varphi - \varphi_i) + a_i \operatorname{Cos}\theta \operatorname{Cos}(\upsilon_i - \varphi + \varphi_i)) \operatorname{Cos}\varphi \quad (1)$$

$$y_P = (R_i \operatorname{Cos}(\varphi - \varphi_i) + a_i \operatorname{Cos}\theta \operatorname{Cos}(\upsilon_i - \varphi + \varphi_i)) \operatorname{Sin}\varphi \quad (2)$$

$$z_P = H_i + a_i \operatorname{Sin}\theta \quad (3)$$

$$dl_i = \vec{a}_\varphi(R_i \operatorname{Cos}(\varphi - \varphi_i) + a_i \operatorname{Cos}\theta \cdot \operatorname{Cos}(\upsilon_i - \varphi + \varphi_i))d\varphi + \vec{a}_\theta a_i d\theta + \vec{a}_\rho d\rho = \vec{a}_x dl_{ix} + \vec{a}_y dl_{iy} + \vec{a}_z dl_{iz} \quad (4)$$

The dot product of the unit vectors of this coordinate system and the Cartesian coordinate system using the projection of the unit vectors of the two mentioned coordinate systems on the x-y plane are presented in Table 1. The longitudinal components of the ith ring element in the Cartesian coordinate system are obtained using Table 1 as in Equations (5)–(7).

Since the ith ring's geometric loci is given by $\rho = a_i$, the longitudinal components of the ith ring by substitution of $d\rho = 0$ can simplify Equations (4) to (7). Furthermore, the relation between θ and φ for the ith ring and the differential of φ, using Fig. 4, can be expressed as Equations (8) and (9). The dependency of the presented

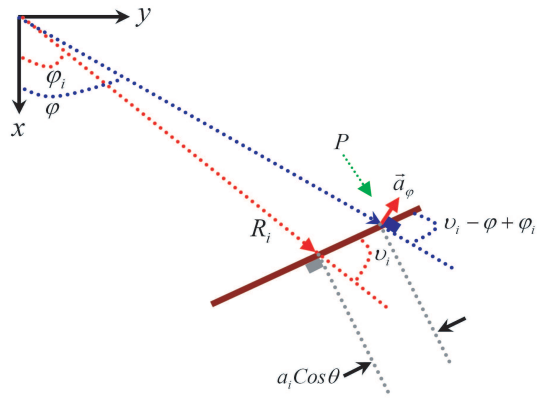

Figure 4. The projection of the ith ring on the x-y plane.

Table 1. The dot product of the vectors for the two mentioned coordinated system.

$\vec{a}_x \bullet \vec{a}_\theta$	$-\operatorname{Sin}\theta \operatorname{Cos}(\upsilon_i - \varphi + \varphi_i) \operatorname{Cos}\varphi$
$\vec{a}_x \bullet \vec{a}_\varphi$	$-\operatorname{Sin}\varphi$
$\vec{a}_x \bullet \vec{a}_\rho$	$\operatorname{Cos}\theta \operatorname{Cos}(\upsilon_i - \varphi + \varphi_i) \operatorname{Cos}\varphi$
$\vec{a}_y \bullet \vec{a}_\theta$	$-\operatorname{Sin}\theta \operatorname{Cos}(\upsilon_i - \varphi + \varphi_i) \operatorname{Sin}\varphi$
$\vec{a}_y \bullet \vec{a}_\varphi$	$\operatorname{Cos}\varphi$
$\vec{a}_y \bullet \vec{a}_\rho$	$\operatorname{Sin}\varphi \operatorname{Cos}(\upsilon_i - \varphi + \varphi_i) \operatorname{Cos}\theta$
$\vec{a}_z \bullet \vec{a}_\theta$	$\operatorname{Cos}\theta$
$\vec{a}_z \bullet \vec{a}_\varphi$	0
$\vec{a}_z \bullet \vec{a}_\rho$	$\operatorname{Sin}\theta$

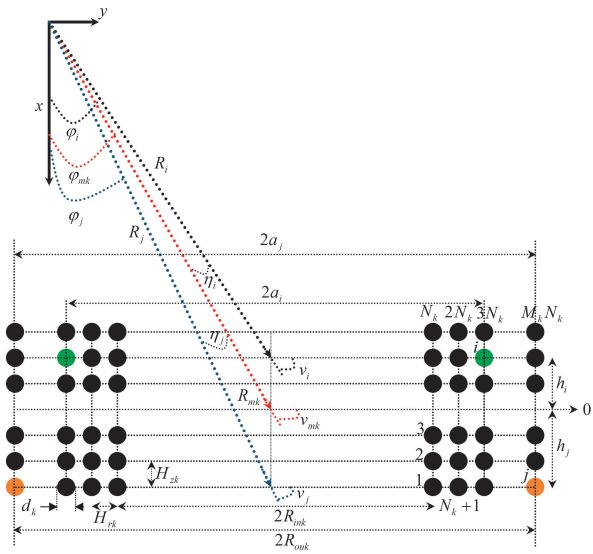

Figure 5. Latitudinal cross-section of the Kth SC with a rectangular section.

equations on the geometrical parameters of the ith ring shows that the relation between the geometrical parameters of the Kth SC of the MTC and the geometrical parameters of the rings of the same SC should be defined. In Fig. 5, the latitudinal cross-section of the Kth SC of the MTC with the geometrical parameters of this coil, i.e., υ_{mk}, R_{mk}, φ_{mk}, and H_{mk} is shown. In this figure, the numbers on each ring indicate

the sequence of the rings connected in series.

$$\begin{aligned} dl_{ix} &= dl_i \cdot \vec{a}_x = -a_i \operatorname{Sin}\theta \operatorname{Cos}(\upsilon_i - \varphi + \varphi_i) \cdot \operatorname{Cos}\varphi d\theta \\ &\quad + \operatorname{Cos}\theta \operatorname{Cos}(\upsilon_i - \varphi + \varphi_i) \cdot \operatorname{Cos}\varphi d\rho \\ &\quad - \operatorname{Sin}\varphi(R_i \operatorname{Cos}(\varphi - \varphi_i) + a_i \operatorname{Cos}\theta \operatorname{Cos}(\upsilon_i - \varphi + \varphi_i))d\varphi \quad (5) \\ dl_{iy} &= dl_i \cdot \vec{a}_y = -a_i \operatorname{Sin}\theta \operatorname{Cos}(\upsilon_i - \varphi + \varphi_i) \operatorname{Sin}\varphi \cdot d\theta \\ &\quad + \operatorname{Cos}\theta \operatorname{Cos}(\upsilon_i - \varphi + \varphi_i) \operatorname{Sin}\varphi d\rho \\ &\quad + \operatorname{Cos}\varphi \cdot (R_i \operatorname{Cos}(\varphi - \varphi_i) + a_i \operatorname{Cos}\theta \operatorname{Cos}(\upsilon_i - \varphi + \varphi_i))d\varphi (6) \\ dl_{iz} &= dl_i \cdot \vec{a}_z = a_i \operatorname{Cos}\theta d\theta + \operatorname{Sin}\theta d\rho \quad (7) \\ \varphi &= \varphi_i + \tan^{-1}\left(\frac{a_i \operatorname{Cos}\theta \operatorname{Sin}\upsilon_i}{R_i + a_i \operatorname{Cos}\theta \operatorname{Cos}\upsilon_i}\right) \quad (8) \\ d\varphi &= \frac{-a_i R_i \operatorname{Sin}\upsilon_i \operatorname{Sin}\theta}{R_i^2 + a_i^2 \operatorname{Cos}^2\theta + 2a_i R_i \operatorname{Cos}\theta \operatorname{Cos}\upsilon_i} d\theta \quad (9) \end{aligned}$$

As seen in Fig. 5, the Kth SC of the MTC is composed of $N_k M_k$ rings, where M_k is the number of the layers, and N_k represents the number of rings in each layer. Using the filament current method, if each ring of the Kth SC is modeled as a filament current, then the inductance matrix is $N_k M_k$ by $N_k M_k$. Knowing the dimensional parameters of the Kth SC (M_k, N_k, d_k, H_{zk}, R_{ouk}, R_{ink}) and the geometrical parameters of the same coil (υ_{mk}, R_{mk}, φ_{mk}, H_{mk}), the geometrical parameters of the ith ring, i.e., υ_i, φ_i, R_i, a_i, and H_i, can be derived as Equations (10) to (14). Using the filament current method, the number of rings of the MTC consisting of S SCs is A, as given in Equation (15). Consequently, the inductance matrix of the MTC is A by A.

The relation between the geometrical parameters of each ring of the MTC with the geometrical and the dimensional parameters of the corresponding SCs are given as Equations (10)–(14), when $i = 1, \ldots, A$.

$$\eta_i = \tan^{-1}(h_i \operatorname{Cos}\upsilon_{mk}/(R_{mk} - h_i \operatorname{Sin}\upsilon_{mk})) \quad (10)$$

$$\varphi_i = \varphi_{mk} + \eta_i \quad (11)$$

$$\upsilon_i = \upsilon_{mk} - \eta_i \quad (12)$$

$$R_i = (R_{mk} - h_i \operatorname{Sin}\upsilon_{mk})/\operatorname{Cos}\eta_i \quad (13)$$

$$H_i = H_{mk} \quad (14)$$

$$A = \sum_{i=1}^{S} M_i N_i \quad (15)$$

4. CALCULATION OF THE SELF- AND THE MUTUAL INDUCTANCE OF THE RINGS

In this section, equations for the calculation of the self inductance of one ring and the mutual inductance of two rings of the MTC are presented. Utilizing the Biot-Savart equation, the self-inductance of the ith ring with radius a_i and conductor diameter d can be expressed by (16). Additionally, using Neumann's equation, the mutual inductance between the ith and the jth ring with the geometrical parameters of υ_i, φ_i, R_i, a_i, H_i and υ_j, φ_j, R_j, a_j, H_j can be calculated by (17). The main diagonal elements of the inductance matrices of each solenoidal coil and MTC are calculated using Equation (16), and the other elements are calculated using Equation (17). For instance, $L_{65,23}$ is the mutual inductance between the 65th and the 23th ring, and $L_{35,35}$ indicates the self-inductance of the 35th ring of the MTC.

The inductance matrix and the inductance of the MTC are described by (18) and (19), respectively. It should be added that if the MTC is symmetrical in its structure, and the geometrical and dimensional parameters of SCs are identical, then the inductance matrix of Equation (18) is symmetrical with respect to its main diagonal and can be divided into S^2 sub-matrices.

$$L_{i,i} = \int_0^{a_i-(d/2)} \int_0^{2\pi} \int_0^{2\pi} f(\rho,\theta,\theta')d\rho\, d\theta\, d\theta' \tag{16}$$

$$f(\rho,\theta,\theta') = \frac{\mu\, a_i \rho[\rho\,\mathrm{Cos}\,(\theta-\theta') - a_i]}{4\pi\,[\rho^2 - 2a_i\rho\,\mathrm{Cos}\,(\theta-\theta') + a_i^2]^{1.5}}, \quad i = 1,\ldots,A$$

$$L_{i,j} = \oint_{\rho=a_i} \oint_{\rho=a_j} \frac{dl_i \bullet dl_j}{|r_{ij}|} = \int_0^{2\pi} \int_0^{2\pi} g(\theta_i,\theta_j)d\theta_i d\theta_j \quad i \neq j \tag{17}$$

where

$$g(\theta_i,\theta_j) = \frac{\mu[dl_{ix}dl_{jx} + dl_{iy}dl_{jy} + dl_{iz}dl_{jz}]}{4\pi[(x_i-x_j)^2 + (y_i-y_j)^2 + (z_i-z_j)^2]^{1.5}}$$

$$\begin{aligned} dl_{ix}dl_{jx} = {} & [-a_i\,\mathrm{Sin}\,\theta_i\,\mathrm{Cos}\,(\upsilon_i - \lambda_i + \varphi_i)\,\mathrm{Cos}\,\lambda_i \\ & - \mathrm{Sin}\,\lambda_i(R_i\,\mathrm{Cos}\,(\lambda_i - \varphi_i) + a_i\,\mathrm{Cos}\,\theta_i\,\mathrm{Cos}\,(\upsilon_i - \lambda_i + \varphi_i))\gamma_i] \\ & \cdot [-a_j\,\mathrm{Sin}\,\theta_j\,\mathrm{Cos}\,(\upsilon_j - \lambda_j + \varphi_j)\,\mathrm{Cos}\,\lambda_j \\ & - \mathrm{Sin}\,\lambda_j(R_j\,\mathrm{Cos}\,(\lambda_j - \varphi_j) + a_j\,\mathrm{Cos}\,\theta_j\,\mathrm{Cos}\,(\upsilon_j - \lambda_j + \varphi_j))\gamma_j] \\ dl_{iy}\,dl_{jy} = {} & [-a_i\,\mathrm{Sin}\,\theta_i\,\mathrm{Cos}\,(\upsilon_i - \lambda_i + \varphi_i)\,\mathrm{Sin}\,\lambda_i \\ & + \mathrm{Cos}\,\lambda_i(R_i\,\mathrm{Cos}\,(\lambda_i - \varphi_i) + a_i\,\mathrm{Cos}\,\theta_i\,\mathrm{Cos}\,(\upsilon_i - \lambda_i + \varphi_i))\gamma_i] \\ & \cdot [-a_j\,\mathrm{Sin}\,\theta_j\,\mathrm{Cos}\,(\upsilon_j - \lambda_j + \varphi_j)\,\mathrm{Sin}\,\lambda_j \\ & + \mathrm{Cos}\,\lambda_j(R_j\,\mathrm{Cos}\,(\lambda_j - \varphi_j) + a_j\,\mathrm{Cos}\,\theta_j\,\mathrm{Cos}\,(\upsilon_j - \lambda_j + \varphi_j))\gamma_j] \end{aligned}$$

$$
\begin{aligned}
dl_{iz}\, dl_{jz} &= [a_i \operatorname{Cos}\theta_i] \cdot [a_j \operatorname{Cos}\theta_j] \\
\lambda_i &= \varphi_i + \tan^{-1}(a_i \operatorname{Cos}\theta_i \operatorname{Sin}\upsilon_i / (R_i + a_i \operatorname{Cos}\theta_i \operatorname{Cos}\upsilon_i)) \\
\gamma_i &= \frac{-a_i R_i \operatorname{Sin}\upsilon_i \operatorname{Sin}\theta_i}{R_i^2 + a_i^2 \operatorname{Cos}^2\theta_i + 2a_i R_i \operatorname{Cos}\theta_i \operatorname{Cos}\upsilon_i} \\
\lambda_j &= \varphi_j + \tan^{-1}(a_j \operatorname{Cos}\theta_j \operatorname{Sin}\upsilon_j / (R_j + a_j \operatorname{Cos}\theta_j \operatorname{Cos}\upsilon_j)) \\
\gamma_j &= \frac{-a_j R_j \operatorname{Sin}\upsilon_j \operatorname{Sin}\theta_j}{R_j^2 + a_j^2 \operatorname{Cos}^2\theta_j + 2a_j R_j \operatorname{Cos}\theta_j \operatorname{Cos}\upsilon_j} \\
x_i &= (R_i \operatorname{Cos}(\lambda_i - \varphi_i) + a_i \operatorname{Cos}\theta_i \operatorname{Cos}(\upsilon_i - \lambda_i + \varphi_i)) \operatorname{Cos}\lambda_i \\
y_i &= (R_i \operatorname{Cos}(\lambda_i - \varphi_i) + a_i \operatorname{Cos}\theta_i \operatorname{Cos}(\upsilon_i - \lambda_i + \varphi_i)) \operatorname{Sin}\lambda_i \\
z_i &= H_i + a_i \operatorname{Sin}\theta_i \\
x_j &= (R_j \operatorname{Cos}(\lambda_j - \varphi_j) + a_j \operatorname{Cos}\theta_j \operatorname{Cos}(\upsilon_j - \lambda_j + \varphi_j)) \operatorname{Cos}\lambda_j \\
y_j &= (R_j \operatorname{Cos}(\lambda_j - \varphi_j) + a_j \operatorname{Cos}\theta_j \operatorname{Cos}(\upsilon_j - \lambda_j + \varphi_j)) \operatorname{Sin}\lambda_j \\
z_j &= H_j + a_j \operatorname{Sin}\theta_j
\end{aligned} \tag{18}
$$

$$
L = \begin{bmatrix} L_{1,1} & L_{1,2} & \dots & L_{1,A} \\ L_{2,1} & L_{2,2} & \dots & L_{2,A} \\ \dots & \dots & \dots & \dots \\ L_{A,1} & L_{A,2} & \dots & L_{A,A} \end{bmatrix}_{A \cdot A}
$$

$$
L_{MTC} = \sum_{i=1}^{A} \sum_{j=1}^{A} L_{i,j} \tag{19}
$$

This symmetry can significantly reduce the computation time of the inductance of the MTC. By replacing each sub-matrix with the sum of all the elements of the same sub-matrix, the size of matrix in Equation (18) can be made S by S. In that case, the main diagonal and the other elements of the resulting matrix are the self and the mutual inductance of the SCs, respectively.

5. COMPARING THE ANALYTICAL AND EMPIRICAL RESULTS OF THE SELF- AND THE MUTUAL INDUCTANCE OF THE RINGS

MATLAB® m-files are used to simulate the self- and the mutual inductance of the rings. Numerical integrations of Equations (16) and (17) are performed using the extended three-point Gaussian algorithm [16]. In [17, 18], the self-inductance of a flat ring with radius $a_i = a$ and conductor diameter d is calculated using Equation (20). For instance, the self-inductance of a flat ring with a radius of 200 cm and a conductor diameter of 2 cm using the empirical tables is reported as 14.1441 μH. In Fig. 6, this value and its corresponding percent error is

compared with that obtained from Equation (16) versus n, the number of divisions in the integral domain.

$$L_{i,i} = \mu_0 a[Ln(16a/d) - 1.75] \quad [H] \tag{20}$$

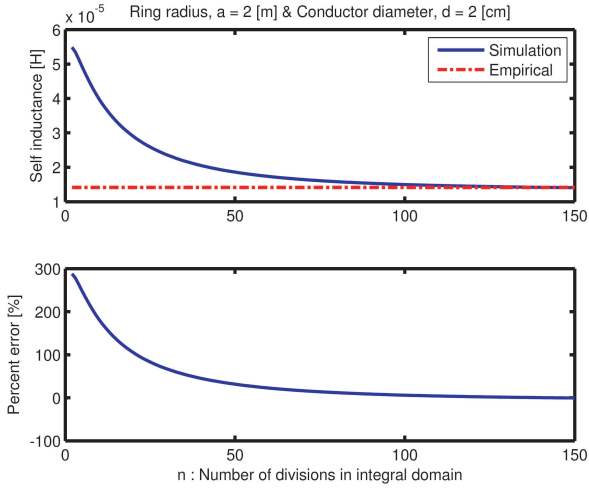

Figure 6. Comparing the analytical and empirical results [17, 18] for the self-inductance of the flat ring.

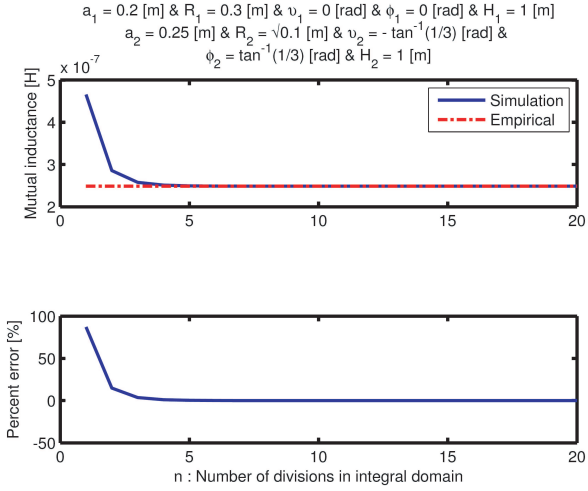

Figure 7. Comparing the analytical and empirical result [19] for the mutual inductance of the flat rings.

In [19], the empirical result of the mutual inductance between two flat rings with radii of 20 and 25 cm and with a center-to-center distance of 10 cm using the empirical tables is reported as 0.24879 μH. In order to compare the empirical and analytical results for the same conditions, the geometrical parameters of the two rings are obtained as in Equation (21). Fig. 7 compares the analytical and empirical results and shows the percent error between them versus n.

$$\begin{aligned} &a_1 = 0.2\,[\mathrm{m}], \quad a_2 = 0.25\,[\mathrm{m}], \quad R_1 = 0.3\,[\mathrm{m}], \\ &R_2 = \sqrt{0.1}\,[\mathrm{m}], \quad \upsilon_1 = 0\,[\mathrm{rad}], \quad H_2 = 1\,[\mathrm{m}] \\ &\upsilon_2 = -\tan^{-1}(1/3)\,[\mathrm{rad}], \quad H_1 = 1\,[\mathrm{m}], \\ &\varphi_1 = 0\,[\mathrm{rad}], \quad \varphi_2 = \tan^{-1}(1/3)\,[\mathrm{rad}] \end{aligned} \tag{21}$$

From Figs. 6 and 7, one can see that the optimum values of n to obtain the minimum percent error and the simulation time in calculating the self and the mutual inductance of rings occur at $n = 100$ and $n = 5$, respectively. These values indicate that the computation time of self-inductance is 400 times more than that of the mutual inductance. Additionally, according to Maxwell, if the radius of the curvature of the ring is larger than the dimensions of the transverse section of the conductor, the equation of the mutual inductance between two rings can be used to calculate the self-inductance of the ring [20]. This significantly reduces the computation time of MTC inductance.

6. A COMPARATIVE STUDY BETWEEN FEM AND ANALYTICAL RESULTS

The FEM is a numerical and computer-based technique for solving a variety of practical engineering problems that arise in different fields. It is recognized by developers and users as one of the most powerful numerical analysis tools ever devised to analyze complex problems in engineering. Because of its diversity and flexibility as an analytical tool, it is receiving much attention in engineering schools and in industry [21].

In this section, the inductances of SCs are obtained using FEM as one of the dimensional parameters (H_z, H_r, R_{in}) are varied. Then, the obtained results are compared with the corresponding analytical results. The dimensional parameters of the SC, including M, N, d, H_z, H_r, R_{in}, are given in Table 2. Using the optimum values of n to calculate the integrations in Equations (16) and (17), the inductance of the SC is calculated as 757.1673 μH. Table 2 shows that the maximum error between the FEM and the analytical results

is less than 0.2%. This error may be due to the mesh size and the value of n. Fig. 8 shows the implemented model of the SC using FEM software. As seen in this figure, because the SC has a symmetrical axis, it is enough to mesh only half of the SC in FEM analysis. Fig. 9 compares the FEM and the analytical results of the inductance of the SC with the geometrical parameters $\upsilon_m = 0$, $R_m = R_{in}$, $\varphi_m = 0$ and $I = 1\,\mathrm{kA}$.

The measured average error is less than 0.2%. As seen in Fig. 10, the inductance of the SC increases when H_r, R_{in} increases (see Figs. 9(a) and (b)), and it decreases as H_z increases (see Fig. 9(c)). In other words, when H_r and R_{in} increase, the variation rate of the self- and mutual inductances of the rings of the SC will be positive; however, when H_z increases, the variation rate will be negative. Moreover, comparing Figs. 9(a) and (b) shows that the increase of H_r has more impact on the variation rate than the increase of R_{in}.

Table 2. Dimensional parameters and comparison of the analytical and FEM results of the inductance of the SC.

Dimensional parameters of the solenoid coil		FEM result	Analytical result
M	8	755.656 [μH]	757.1673 [μH]
N	10		
d	1.6 [mm]		
H_z	2.1 [mm]		
R_{in}	40 [mm]		
H_r	2.3 [mm]		

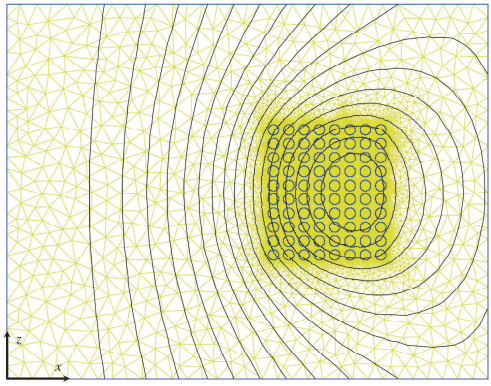

Figure 8. The implemented model of the SC using FEMM software.

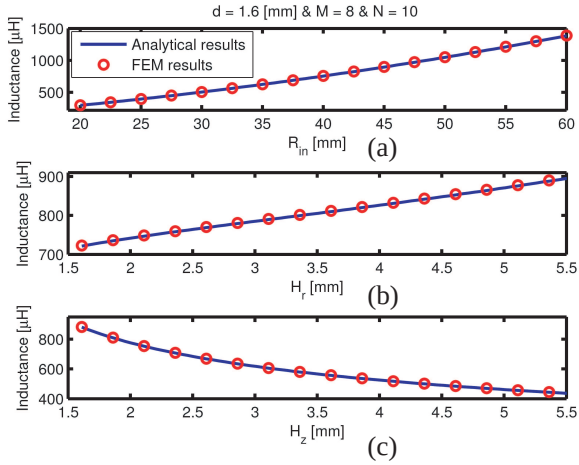

Figure 9. Comparison between the FEM and the analytical results of the inductance of the SC.

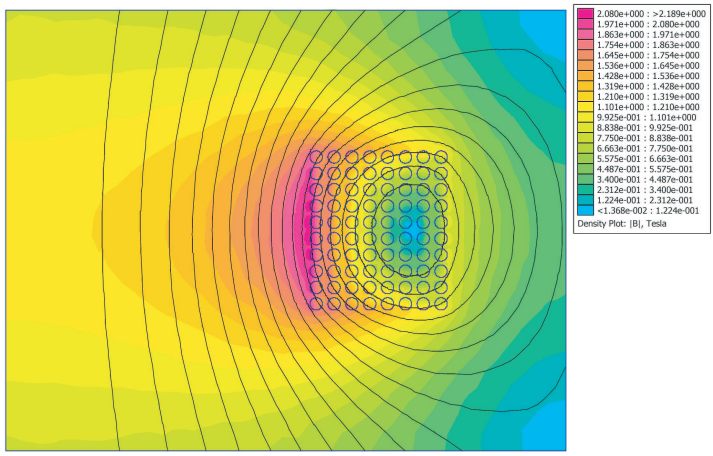

Figure 10. The magnetic flux density of the SC.

Figure 10 shows the magnetic flux density of the SC. As seen in this figure, the magnetic flux density is concentrated in the inner layer, i.e., $M = 1$. Additionally, Fig. 11 confirms that the magnetic flux density concentration occurs in the inner layer. Note that the magnetic flux density in Fig. 11 is drawn between the 5th and 6th ring.

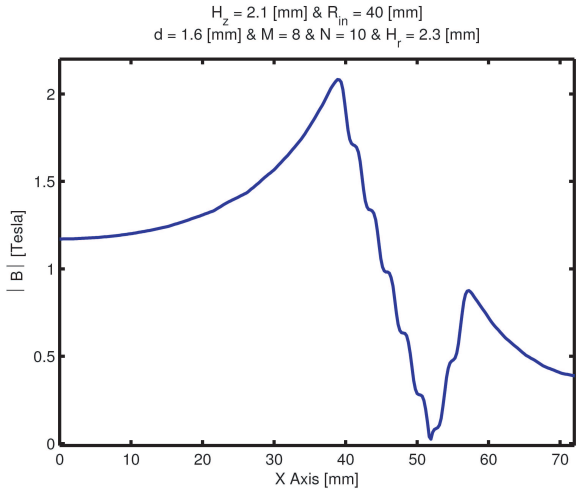

Figure 11. The magnetic flux density between the 5th and 6th rings.

7. CONCLUSION

Theoretical studies of the MTC are still in the development stage. Since the optimal design of the MTC with different objective functions, such as the maximization of the stored magnetic energy, the minimization of leakage flux, the stabilization of tokamak reactors, and the elimination of stress, requires anaccurate calculation of the inductances of this coil, in this article, we first derive the analytical equations of the inductances of this coil. Similar to that of the helical toroidal coil, the calculation of the inductance of the MTC can be employed to predict transient state behavior, find the equivalent electrical circuit, and identify the electrical elements of the equivalent electrical circuit of the MTC.

In this paper, equations for the calculation of the inductance of the MTC are presented. Additionally, the behavior of the analytical results of the inductance of the SC is studied when its dimensional parameters are varied. The analytical results are carried out using MATLAB®. To validate the presented equations for the SC, FEM is used. The analytical, empirical, and FEM results are compared. This comparison shows that the obtained error is less than 0.2%; therefore, the proposed equations are highly reliable.

REFERENCES

1. Alizadeh Pahlavani, M. R. and A. Shoulaie, "A novel approach for calculations of helical toroidal coils inductance usable in reactor plasmas," *IEEE Trans. on Plasma Science*, Vol. 37, No. 8, 1593–1603, Aug. 2009.
2. Alizadeh Pahlavani, M. R. and A. Shoulaie, "Elimination of compressive stress in helical toroidal coils advanced structure for reactor plasmas," *IEEE Trans. on Plasma Science*, Vol. 37, No. 11, 2166–2177, Nov. 2009.
3. Alizadeh Pahlavani, M. R. and A. Shoulaie, "Behavioral study of stress in toroidal, solenoidal, and helical toroidal coils with similar ring structures for reactor plasma," *International Review of Electrical Engineering*, Vol. 4, No. 1, 146–158, Jan.–Feb. 2009.
4. Romeo, A. and R. P. Garabedian, "Choice of coils for a fusion reactor," *Proceedings of the National Academy of Sciences*, Vol. 104, No. 30, 12250–12252, Jul. 24, 2007.
5. Babic, S. I. and C. Akyel, "New mutual inductance calculation of the magnetically coupled coils: Thin disk coil-thin wall solenoid," *Journal of Electromagnetic Waves and Applications*, Vol. 20, No. 10, 1281–1290, 2006.
6. Akyel, C., S. I. Babic, and M.-M. Mahmoudi, "Mutual inductance calculation for non-coaxial circular air coils with parallel axes," *Progress In Electromagnetics Research*, PIER 91, 287–301, 2009.
7. Akyel, C., S. I. Babic, S. Kincic, and J. P. Lagacé, "Magnetic force calculation between thin circular coils and thin filamentary circular coil in air," *Journal of Electromagnetic Waves and Applications*, Vol. 21, No. 9, 1273–1283, 2007.
8. Shiri, A. and A. Shoulaie, "A new methodology for magnetic force calculations between planar spiral coils," *Progress In Electromagnetics Research*, PIER 95, 39–57, 2009.
9. Koledintseva, M. Y., J. L. Drewniak, T. P. Van Doren, D. J. Pommerenke, M. Cocchini, and D. M. Hockanson, "Method of edge currents for calculating mutual external inductance in a microstrip structure," *Progress In Electromagnetics Research*, PIER 80, 197–224, 2008.
10. Koledintseva, M. Y., J. L. Drewniak, T. P. Van Doren, D. J. Pommerenke, M. Cocchini, and D. M. Hockanson, "Mutual external inductance in stripline structures," *Progress In Electromagnetics Research*, PIER 80, 349–368, 2008.
11. Ravaud, R., G. Lemarquand, and V. Lemarquand, S. I. Babic, and C. Akyel, "Mutual inductance and force exerted between thick

coils," *Progress In Electromagnetics Research*, PIER 102, 367–380, 2010.

12. Zhao, P. and H.-G. Wang, "Resistances and inductances extraction using surface integral equation with the acceleration of multilevel Green function interpolation method," *Progress In Electromagnetics Research*, PIER 83, 43–54, 2008.
13. Wang, H.-G. and P. Zhao, "Combining multilevel Green's function interpolation method with volume loop bases for inductance extraction problems," *Progress In Electromagnetics Research*, PIER 80, 225–239, 2008.
14. Tang, W., X. He, T. Pan, and Y. L. Chow, "Synthetic asymptote formulas of equivalent circuit components of square spiral inductors," *Journal of Electromagnetic Waves and Applications*, Vol. 20, No. 2, 215–226, 2006.
15. Venkov, G., M. W. McCall, and D. Censor, "The theory of low-frequency wave physics revisited," *Journal of Electromagnetic Waves and Applications*, Vol. 21, No. 2, 229–249, 2007.
16. Pennington, R. H., *Introductory Computer Methods and Numerical Analysis*, 4th edition, Macmillan, New York, 1970.
17. Bueno, M. and A. K. T. Assis, *Equivalence between the Formulas for Inductance Calculation*, 357–362, NRC, Canada, 1997.
18. Wheeler, H. A., "Formulas for the skin effect," *Proceedings of the I.R.E.*, 412–424, Sep. 1942.
19. Grover, F. W., *Inductance Calculation Working Formulas and Tables*, 77–87, Dover Publications, Inc, New York, 1946.
20. Maxwell, J. C., *A treatise on Electricity and Magnetism*, Vol. 1, 297, (reprint from the original from 1873, 693), Dover Publications Inc, New York, 1954.
21. Anderson, D. A., J. C. Tannehill, and R. H. Pletcher, *Computational Fluid Mechanics and Heat Transfer*, Hemisphere, Washington, DC, 1984.